Title

ELM control experiments in the KSTAR device

Journal

Nuclear Fusion, 52(11)

ISSN

0029-5515

Authors

Kim, Jayhyun

Jeon, Y-M

Xiao, WW

et al.

Publication Date

2012-11-01

DOI

10.1088/0029-5515/52/11/114011

Peer reviewed

ELM Control Experiments in the KSTAR Device

Jayhyun Kim[1], Y-.M. Jeon[1], W.W. Xiao[2,10], S-.W. Yoon[1], J-.K. Park[3], G.S. Yun[4], J-W. Ahn[5], H.S. Kim[6], H-.L. Yang[1], H.K. Kim[1], S. Park[1], J.H. Jeong[1], M. Jung[1], G.H. Choe[4], W.H. Ko[1], S-.G. Lee[1], Y.U. Nam[1], J.G. Bak[1], K.D. Lee[1], H.K. Na[1], S-.H. Hahn[1], P.H. Diamond[2,11], T. Rhee[2], J.M. Kwon[2], S.A. Sabbagh[7], Y.S. Park[7], H.K. Park[4], Y.S. Na[6], W.C. Kim[1], J.G. Kwak[1] and the KSTAR contributors[1-11]

[1]National Fusion Research Institute (NFRI), Daejeon 305-333, Korea
[2]WCI center for Fusion Theory, NFRI, Daejeon 305-333, Korea
[3]Princeton Plasma Physics Laboratory, P.O. Box 451, Princeton, NJ 08543, USA
[4]Pohang University of Science and Technology, Pohang, Gyungbuk 790-784, Korea
[5]Oak Ridge National Laboratory, Oak Ridge, Tennessee 37831, USA
[6]Seoul National University, Seoul 151-742, Korea
[7]Columbia University, New York, New York 10027, USA
[8]General Atomics, P.O. Box 85608, San Diego, CA 92186-5608, USA
[9]Japan Atomic Energy Agency, Naka, Ibaraki-ken 311-0193, Japan
[10]Southwestern Institute of Physics, P.O. Box 432, Chengdu, China
[11]University of California San Diego, La Jolla, CA 92093-0319, USA

E-mail: jayhyunkim@nfri.re.kr

Abstract. The 4th KSTAR campaign in 2011 concentrated on active ELM control by various methods such as non-axisymmetric magnetic perturbations, supersonic molecular beam injection (SMBI), vertical jogs of the plasma column, and edge electron heating. The segmented in-vessel control coil (IVCC) system is capable of applying $n \leq 2$ perturbed field with different phasing among top, middle, and bottom coils. Application of an $n=1$ perturbed field showed desirable ELM suppression result. Fast vertical jogs of the plasma column achieved ELM pace making and ELMs locked to 50 Hz vertical jogs were observed with a high probability of phase locking. A newly installed SMBI system was utilized for ELM control and a state of mitigated ELMs was sustained by the optimized repetitive SMBI pulse for a few tens of ELM periods. A change of ELM behavior was seen due to edge electron heating although the effect of ECH launch needs supplementary analyses. The ECEI images of

suppressed/mitigated ELM states showed apparent differences when compared to natural ELMy states. Further analyses are on-going to explain the observed ELM control results.

1. Introduction

When compared to low confinement mode (L-mode) which does not have an edge transport barrier (ETB), the high confinement mode (H-mode) in magnetically confined thermonuclear fusion devices exhibits almost a factor of two enhanced confinement and a resulting improvement of stored plasma energy [1]. Since it was discovered during neutral beam injection (NBI) heated discharges in the ASDEX device, achievements of the H-mode have been reported in various types of magnetic fusion devices including tokamaks and stellarators [1, 2]. Therefore, the international thermonuclear fusion reactor (ITER) project considers the ELMy H-mode as its baseline scenario in order to accomplish its major goal, Q=10 where the fusion gain, Q is the ratio of fusion power to auxiliary heating power [3, 4].

In the H-mode phase, formation of edge particle and thermal transport barriers considerably increases the pressure gradient and current density near plasma edge region due to good confinement. The resulting edge pedestal structure periodically suffers abrupt relaxation processes; the so called edge localized mode (ELM) bursts [1]. It is believed that large type-I ELMs are caused by a transient MHD instability originating from an excessively steep edge pedestal [5, 6]. This kind of abrupt relaxation processes could be harmful to plasma facing components (PFCs) of reactor scale devices such as ITER. The expected transient heat loading due to ELM bursts in ITER is twenty times higher than the tolerable level of the ITER PFC materials [7]. As a consequence, it is crucial to reduce the transient heat loading during typical H-mode discharges so as to ensure the life time of PFCs in reactor scale device. Although various approaches have been tried including a fundamental change of operation modes, for instance, a quiescent high confinement mode (QH-mode) [8] or H-mode discharges with small ELMs [9], these regimes with intrinsic small ELMs simply were not found at the ITER relevant parameters in terms of collisionality, density, q_{95}, beta poloidal, and etc. [10]. As a result active ELM control became urgent for ITER. We focused our effort on active ELM control methods [11-13] which aim to ameliorate intrinsic ELMs.

Large ELMs can be continuously avoided by inhibiting the build-up of steep edge pedestals [11] or changing the stability boundary of ELMs [14] through the application of a non-axisymmetric (NA) field to an axisymmetric equilibrium field, even though the underlying mechanisms of the ELM suppression/mitigation are still not clear. In the 2011 Korea Superconducting Tokamak Advanced Research (KSTAR) [15] campaign, an n=1 NA field enabled full suppression of ELMs in intrinsically ELMy H-mode discharges for several hundreds of miliseconds which correspond to factor of three longer than the energy and particle confinement times [16]. In addition, shallow particle deposition by the SMBI showed apparent ELM mitigation in KSTAR H-mode discharges. Although the ELM

mitigation by the SMBI was already reported in the HL-2A experiments [17], the influence time of the SMBI in KSTAR experiments is about a factor of ten longer than that of the HL-2A [18]. Furthermore, direct heating or current drive in the pedestal region [19, 20] which influences the stability boundary of ELMs is regarded as a candidate ELM control method as well. Electron cyclotron (EC) heating at 110 and 170 GHz, which deposited energy near the edge pedestals of KSTAR H-mode discharges, produced observable changes.

On the other hand, the ELM induced energy loss of an individual ELM burst can be decreased by increasing the ELM frequency, since it is observed that the ELM induced energy loss per ELM is inversely proportional to the ELM frequency [21]. The increase of ELM frequency is technically produced by transient perturbations which are able to directly influence edge pedestals [12, 22-24]. Pellet injection and vertical jogs of plasma column have shown hopeful results in so called ELM pace-making, and they are valued as promising control knobs for raising the ELM frequency from its intrinsic value. ELMs were intentionally triggered by vertical jogs of the plasma column at certain phases of the jogs in the 2011 KSTAR H-mode discharges.

Typical characteristics of ELMs in the KSTAR H-mode discharges are briefly described in section 2. Section 3 reports the detailed results of ELM control experiments in the 2011 KSTAR campaign with explanations of the experimental set-ups of the applied methods. In section 4, the results of the previous sections are summarized and the direction for future experiments on the aforementioned ELM control methods is discussed.

2. Characteristics of ELMs in the KSTAR H-mode discharges

In the 2011 KSTAR campaign, we observed three different types of ELMs which were discriminated by ELM size $\Delta\bar{n}_e/\bar{n}_e$, ELM frequency f_{ELM}, and confinement quality (H-factor) [25, 26]. The first and second types of ELMs were large type-I ELMs ($\Delta\bar{n}_e/\bar{n}_e$~1-4 %), with low ELM frequency (f_{ELM}~10-50 Hz) and good confinement ($H_{98(y,2)}$~0.9-1), and medium size ELMs ($\Delta\bar{n}_e/\bar{n}_e$ <1 %), with higher ELM frequency (f_{ELM}~50-250 Hz) and poorer confinement ($H_{98(y,2)}$~0.7-0.8), respectively. This is similar to the observation of type-I and type-III ELMs in [27]. The last type of observed ELMs was a mixture of large type-I ELMs and small frequent ELMs on the background. The mixed type showed good confinement ($H_{98(y,2)} \geq 1$).

We investigated a relation between auxiliary heating power and the frequency of large ELMs [26]. It exhibited the positive proportionality which is a typical characteristic of type-I ELM. In addition, large type-I ELMs had an inverse proportionality between ELM size and ELM frequency. However, medium size ELMs did not show the inverse proportionality between ELM size and ELM frequency. During the period of mixed type ELMs, large ELMs and small ELMs followed the aforementioned characteristics of large type-I ELMs and medium size ELMs, individually.

In figure 1, the time traces of D_α signal, stored energy, and H_{89p} factor are depicted for the reference (#5953) and the SMBI applied discharge (#6352). Discharge #5953 shows a relatively lower confinement (H_{89p}~1.6) with higher ELM frequency (f_{ELM} >50 Hz). Therefore, we suggest that the type of ELMs in #5953 was the aforementioned medium size ELMs, possibly type-III ELMs. In the KSTAR discharge #6352, initial ELM free phase was ended before t=2.3 s and the first SMBI pulse was injected at t=2.7 s. Thus, the ELMs between 2.5 s and 2.7 s were a good reference for the ELM mitigation experiment by the SMBI. As shown in figure 1(d), the confinement factor H_{89p} was higher than 2.0 and D_α peaks represented a mixture of large and small peaks. The detailed change of ELMs by the SMBI will be described in section 3.2.

Since marginal heating power and plasma control issue prevented to make type-I ELM period sufficiently long in the 2011 KSTAR campaign, the ELM control experiments were mainly conducted on the type-III like medium size ELMs and the mixed type ELMs.

3. Applied ELM control methods and their results

3.1 Non-axisymmetric magnetic field perturbation

Since the design phase of the KSTAR device, the installation of segmented in-vessel control coils has been considered for vertical instability control, intrinsic error field correction, and resistive wall mode suppression [28]. Owing to the segmented geometry of the IVCC, some parts of the IVCC act as axisymmetric ring type coils used for plasma position control while other parts form so called picture frame type coils for generating a NA field as depicted in figure 2. In the poloidal direction, by connecting the neighboring IVCC bundles, we can make three pairs of picture frame coils designated as top, middle, and bottom field error correction (FEC) coils. Each IVCC bundle is toroidally divided into four segments thus the maximum applicable toroidal mode number, n of an NA field is two. The parity of each picture frame, *i.e.* the outward or inward radial direction of the generated field and the resulting toroidal phase of the NA field are selected by connections among segmented coil parts and their attached power supply. Similarly, the relation among the toroidal phases of the top, middle, and bottom FEC coils determines the poloidal phasing, *i.e.*, the pitch of the resulting NA field to the equilibrium field.

For responding to an urgent issue related to the design of ITER ELM control coils [29], a total of three unipolar power supplies were installed for each FEC coil group, *i.e.*, the top, middle, and bottom FEC coils during the upgrade period before the 2011 campaign. The maximum current of each power supply was 1.8 kA/turn. The number of turns in each picture frame coil is two therefore the actual maximum current becomes 3.6 kA*turn.

In the 2011 KSTAR experiments, by applying an n=1 NA field perturbation, we observed different ELM control effects varying from full suppression of ELMs to the intensification of ELMs, depending on the poloidal phasing of the FEC coils. The various results of n=1 NA field applications are

summarized in table 1. The full suppression of ELMs was achieved with n=1, +90 poloidal phasing of the NA field. Figure 3 represents two similar KSTAR H-mode discharges except for the application of an NA field for the comparison of the NA field effect [16]. As shown in figures 3(b) and 3(c), it was observed that the ELM burst signature in the D_α signals completely disappeared during ~600 ms. One thing noteworthy in the figure is that the intensified ELMs emerge before the ELM suppression period but after the power supplies of the FEC coils are turned on. This could be related to the early increase of the middle FEC coil current prior to the other two off-midplane coils, due to a synchronization problem of the FEC control system. An experiment using the middle FEC coil alone supported the idea of ELM intensification by the middle FEC coil though the intensification mechanism needs further investigation. The ELM intensification phase exhibited almost 10 % drops of plasma parameters including line-averaged electron density, stored plasma energy, and core rotation velocity, compared with the reference discharge #5953, while the drops of electron and ion temperatures were not quite apparent during this phase. On the other hand, during the following ELM suppression phase, the stored plasma energy and core rotation velocity became stationary as shown in figures 3(g) and 3(h).

It has been routinely observed that there was an evolution of filament structures in the edge pedestal region during ELM events by the ECEI system since the 2010 KSTAR campaign [30]. The ECEI images taken from the ELM control experiments by NA field perturbations depicted the differences among various ELM phases such as an intrinsic ELM phase, an intensified ELM phase, and a suppressed ELM phase. As shown in figure 4 [31], the filament structures were not seen clearly during the ELM suppression phase while the intrinsic and intensified ELM phases showed the apparent filament structures [31]. Moreover, the filament sizes or poloidal mode numbers of the filaments were much different between the intrinsic and intensified ELM phases. The difference of the filament structures could be related to a modification of ELM driving modes due to the change of ELM stability boundaries by the application of NA field perturbations.

A series of experiments was conducted in order to investigate the minimum level of the NA field required for ELM suppression by varying the FEC coil current. Figure 5 represents the ELM control results depending on the level of FEC coil current. ELMs began to be mitigated from 1.5 kA*turn and completely suppressed above 3.0 kA*turn [16]. The investigation of the minimum NA field level has an importance in the application of low n NA fields since it heavily correlates with plasma mode locking. Occasionally an H-L back transition and subsequent plasma mode locking were observed with the FEC configuration of n=1, +90 poloidal phasing. The difference of edge electron temperature between the ELM suppression case and the unfavorable mode locking case gave some information on the role of edge collisionality. However, detailed analysis is required with edge profile measurements for understanding the underlying physics. During the next KSTAR campaign, a more systematic study will be carried out to find the optimal level of FEC coil current which achieves ELM suppression but avoids locking [32].

3.2 Supersonic molecular beam injection

In this section, we will report the results of ELM mitigation which were obtained by shallow particle deposition in the H-mode pedestal utilizing the newly installed SMBI system. ELM control experiments by pulsed fueling have been carried out in many tokamaks. The most widely-used technique is so called ELM pace-making by pellet injection [22, 23]. To alter ELM characteristics and stability, fueling or impurity seeding should reach sufficiently deep into the pedestal region thus the capability of conventional gas puffing for the purpose of ELM control is rather restrictive [22]. On the other hand, both SMBI and pellet injection can deliver direct perturbations into the pedestal region owing to their speed and size.

It has been generally accepted that pellet injection, which penetrates deeply into or beyond the pedestal, directly causes MHD instabilities, and thus a resulting ELM burst per pellet injection [23, 33]. However, in the case of the SMBI, the penetration depth is shallower than that of pellet injection; therefore SMBI needs not immediately provoke an ELM burst [17, 18]. We suggest that shallow particle deposition by a SMBI changes the local characteristics of the pedestal transport dynamics and the local density profile structure, and consequently alters the ELM dynamics. It is noteworthy that each pellet injection is highly coherent with individual ELM triggering but the SMBI pulses are not directly correlated with individual ELMs.

A train of three SMBI pulses achieved the mitigation of large ELMs in KSTAR as shown in figure 6 for KSTAR discharge #6376, with similar plasma parameters to KSTAR discharge #6352 [18]. The type of ELMs was altered from large ELMs to small ones after the SMBI pulses. The SMBI injection sequence is shown in figure 6(f). Three pulses (τ_{SMBI}~8 ms, 1 MPa) are injected in this shot. The corresponding change of the key parameters is introduced in figures 6(a) to 6(e). Figure 6(a) depicts the plasma core (red curve) and edge temperature (blue curve), respectively. A drop of the temperature is clear when a SMBI pulse is injected, as shown by the dotted lines. The edge temperature decrease rate with time due to SMBI is faster than that in the core plasma, which means the cold SMBI particle source is deposited in the plasma edge rather than in the core. In figures 6(b) and 6(c), there are responses at the plasma current I_p and line-averaged density n_e. The plasma current drops and density increases (Δn_e~$0.5\text{x}10^{19}$ m^{-3}) just after the SMBI pulses. The SMBI influence time τ_I can be maintained during several tens of ELM periods as shown by the D_α signal in figure 6(d) using double arrows. τ_I of pulse A and B are 280 ms and 320 ms, respectively. The red curve in figure 6(e) is the global stored energy, W_p in kJ. Some modest decay after SMBI pulse injection is observed at 2.7 s in the global stored energy for KSTAR discharge #6376. In figure 6(e), the blue squares are the experimental results measured by x-ray imaging crystal spectroscopy (XICS) [34] of the toroidal rotation evolution with time. After each pulse injection, the plasma toroidal rotation decreases and then recovers. The change of ELM types was consistent with the drop of measured stored energy, *i.e.*, slight degradation in plasma confinement. It is known that the type-I-like large ELMy state shows

better confinement than the type-III-like small ELMy state. In addition, toroidal rotation decreases due to SMBI have been observed, and is consistent with a faint degradation of the global confinement in the experiments of ELM mitigation by SMBI.

Figure 7 shows changes of edge pedestal density fluctuations during the ELM mitigation by SMBI [18], as obtained from experimental measurements using the beam emission spectroscopy (BES) system [35] for KSTAR discharge #6352 at two different positions. The density fluctuations in figure 7(a) are measured close to the pedestal top. In figure 7(b), the measurement is outside of the half pedestal width. In this figure, there is not a strong effect on the density fluctuations in figure 7(a) as compared to figure 7(b). For figure 7(a), that means the particle source due to a SMBI pulse did not deeply penetrate to the top of the pedestal. However, for figure 7(b), results suggest the SMBI can penetrate to this position and make the density fluctuations increase in the high frequency region with the confinement decay.

A simplified model, which uses a diffusive bi-stable cellular automata model, was applied to understand the shallow particle deposition effect of SMBI on ELM mitigation [36]. Through the sand-pile model study, it was seen that shallow particle deposition induced frequent small ejection events which prevented formation of large crashes. For the deep particle deposition, the mitigation effect of large crashes was rarely observed. The basic model is described in reference [37] and consists of a sand pile with an ejecting boundary on one side, a bi-stable toppling rule, noise-driven scattering to emulate collision diffusion, and an ultimate upper hard threshold on the occupation density profile. The bi-stable toppling rule for the pile incorporates aspects of L and H phase turbulent transport. The hard threshold emulates an upper limit on profile steepness, as in a $\bigtriangledown P_{\mathrm{crit}}$ for MHD instabilities, frequently associated with ELMs. ELMs occur when the entire edge pedestal region is populated up to the hard threshold limit, and occur as ejection events driven by avalanches, which span the full pedestal cross-section. The trends indicated by this simplified model study are all qualitatively consistent with the experimentally observed trends, and suggest that shallow SMBI deposition into the pedestal mitigates ELMs by reducing the population of large avalanche transport events, while increasing the number of smaller events. The simplified model also predicts pedestal gradients flattening near the deposition position [36]. Figure 8 shows changes of the filament structures by the shallow SMBI depositions outside of the half pedestal width [18]. Sizes of the filament structures during intrinsic ELM phase are decreased by 1st SMBI pulse but the initial filament structures almost recover after the SMBI influence time τ_{I}. Then 2nd SMBI pulse reproduces again the similar filament structures achieved by the 1st SMBI pulse. It experimentally supports the prediction of the sand-pile model in explaining the mechanism of large crash prevention. Based on above experimental observation of ELM mitigation by SMBI, we expect the model to apply to both the Peeling-Ballooning model and also edge particle transport driven relaxation [17, 37].

3.3 Vertical jogs of plasma column

It is thought that the effect of vertical jogs on ELM triggering is due to the change of edge current by inductive motion of plasma column from the result of a TCV ELM pacing experiment [12]. However, there still exist other possible explanations of this ELM trigger mechanism like the sudden deformation of equilibrium after observing the contradictory timing of ELM triggering in ASDEX-U experiment [13, 38].

In order to apply fast vertical jogs from a plasma equilibrium position, we programmed a sawteeth-shaped waveform in the vertical position reference of plasma control system (PCS) [39]. As briefly described in section 3.1, the axisymmetric part of the IVCC produced an appropriate radial field which was superposed with the equilibrium field according to the PCS command. The experiment aimed to lock the ELM frequency to the frequency of vertical jogs by varying the amplitude, velocity, and frequency of vertical jogs. By doing this, we studied basic characteristics of vertical jogs such as the ELM trigger timing in KSTAR discharges.

As depicted in figure 9, the ELM trigger timing was successfully locked to the phase of vertical jogs. The relatively moderate vertical jogs, ~25 mm peak-to-peak amplitude with 50 Hz frequency showed almost exact triggering of ELMs when the plasma moved away from the lower x-point with its maximum speed. The drops of edge electron temperature and line-averaged density were well synchronized with D_α bursts as depicted in figures 9(c) and 9(d).

The reconstructed equilibrium of the reference plasma had an almost double null or slightly lower single null configuration [40]. Therefore the required level of the vertical jogs for ELM triggering seems to be somewhat large when compared with the result from other similar devices [13]. It is worthwhile mentioning that the phase of the actual excursion exhibited an almost out-of-phase behavior with the programmed phase. After deliberately comparing the measured vertical position of the plasma column with non-magnetic diagnostics such as the soft x-ray signal and the broad peak of the D_α signal, we concluded that the phase of the magnetically measured vertical position in the PCS was coincident with the measurements of the aforementioned non-magnetic diagnostics.

When we increased the excursion amplitude in order to oscillate the equilibria between lower single null (LSN) and upper single null (USN) configurations, multiple ELM triggering phenomena occurred. Figure 10 presents multiply triggered ELMs within a single period of a vertical jog. The first ELM was triggered when the plasma reached its lowest position. It did not appear in the previous moderate excursion case. The second and third ELMs happened near the maximum upward speed as already observed in the moderate excursion case. Furthermore, ELMs were triggered only around the LSN configuration although the plasma periodically oscillated between LSN and USN configurations with a very similar excursion level and speed. It was expected there would be different filament structures among the multiple ELMs but the difference of the filament structures was indistinct due to the low signal-to-noise (SN) ratio of ECEI pictures with 170 GHz ECCD power. However, the up-down asymmetric activities of the filaments were identified from the ECEI pictures as expected.

On the other hand, we could not synchronize ELM bursts to 100 Hz vertical jogs. The intrinsic

ELM frequency was measured to be 30~50 Hz even though the bursting timings were somewhat irregular. Comparing with the 50 Hz frequency case, a slight decrease of the excursion amplitude (~20 mm peak-to-peak) was observed with the same excursion amplitude of the PCS command. In the next campaign, we will test a LSN configuration as a target equilibrium to achieve ELM pace-making in higher vertical jog frequencies.

3.4 Edge electron heating

A perturbation on pedestal plasma pressure or current is one of the envisaged techniques for control of ELMs. The well-known 'pellet injection' is a good candidate to trigger ELMs by perturbing the density locally in the pedestal region [24]. On the other hand, there is also possibility of ELM control by direct heating or current drive in the pedestal region [20] which will influence the P-B stability boundary of the ELM. The main heating schemes are ECH, ECCD, and lower hybrid current drive (LHCD) for the local heating and/or current drive in the narrow width of the pedestal which is typically a few centimeters in the KSTAR discharges. In the 2011 KSTAR campaign, the initial experiments of pedestal ECH/ECCD have been done with both gyrotrons with frequencies of 170 GHz and 110 GHz, respectively. Within the limitations of ECH power, the optimal configuration heating on both the low- and high-field sides at the same time is possible by proper tuning of the toroidal magnetic field.

The calculations of heat deposition are based on a ray-tracing code, the TORAY-GA code [41], assuming parabolic profiles of electron temperature and density. The maximum available EC power available is 0.3 MW for 110 GHz and 0.6 MW for 170 GHz, respectively. Power from both gyrotrons is launched at the low field side about 0.2 m below the midplane. Setting up the toroidal field at plasma center as B_{T0}=2.3 T and tilting the mirrors toroidally and poloidally targeting the upper region above the midplane, it is possible to deposit EC power both at the inboard and the outboard pedestal regions simultaneously near the position of the pedestal top thus maximizing pedestal heat deposition. In this case, the power from the 110 GHz gyrotron could be deposited at the upper outer region around ρ_{pol} ($\propto \Psi^{1/2}$)~0.8 and the power from the 170 GHz gyrotron could be deposited at upper inboard side around ρ_{pol}~0.9. The calculated deposition of ECH power in the pedestal is partly confirmed by the measurements of heat pulse propagation using ECE radiometers. The ECE edge channels drop first after turn-off of the EC power and also the modulated ECH confirms the pulse propagation from the pedestal region to the core. In addition, the change of the edge ECE is larger than that of the core and this supports the observation that the ECH power is deposited locally in the pedestal regions.

The effect of pedestal ECH is shown in figure 11. In KSTAR discharge #6313, after the L-H transition, ECH was injected for the period t=2.6-3.1 s (P_{ECH} is shown in the first box of figure 11). The ELM frequency increased during the ECH injection as shown the D_α trace. The f_{ELM} before and after the ECH injection was about 20~30 Hz and during the ECH, f_{ELM} increased up to 40 Hz, which confirms the potential of pedestal ECH for ELM control. In addition, the line-averaged electron

density decreased, suggesting a change of the particle transport in the pedestal region. The central toroidal rotation, V_T is also decreased. However, the stored energy did not change significantly and ΔW_{ELM} was roughly the same before and during ECH. This may be due to the additional power from ECH in the pedestal. Not only f_{ELM} increased but also ΔW_{ELM} did not decrease as the f_{ELM} increases. The effect of current drive was investigated by changing the parallel index of incident ECH beam, but the effect of CD was not discernible. In the next campaign, the effect of ECCD will be further investigated by optimizing the ECCD efficiency.

4. Discussion and summary

Since the first plasma in 2008, the performance of KSTAR plasma has consistently improved. By achieving H-mode discharges [42], a main baseline scenario of ITER, the KSTAR device became ready to contribute to unsolved issues in the thermonuclear fusion area. The 4th campaign in 2011 concentrated on the control of ELMs during the H-mode phase, since this is one of the most urgent issues for ITER machine safety and lifetime [7].

The n=1 NA field perturbation presented different ELM control effects varying from full suppression of ELMs to the intensification of ELMs, depending on the poloidal phasing of the FEC coils. Among the results, n=1, +90 poloidal phasing of the NA field achieved the full suppression of ELMs. It appeared that electron and ion temperatures were little affected by the NA field perturbation regardless of its poloidal phasing. However, plasma density, stored energy, and toroidal rotation exhibited almost 10 % drops during the intensified ELM phase. The dropped plasma density was increased again during the following ELM suppression phase, while the stored energy and the toroidal rotation were maintained at the dropped levels. A systematic study of different ELM characteristics, depending on the spectra of NA fields, will enlarge our understanding of ELM control by NA field perturbation, with already known parameters such as q_{95} windows and edge collisionality. Furthermore, ELM suppression through n=1 NA field perturbation by in-vessel coils might provide the possibility of extension of ELM control by external coils because of the simpler field structure of n=1 NA field, compared to other n>1 cases, in addition to the JET result [32].

The SMBI achieved remarkable ELM mitigation in the KSTAR H-mode discharges as well as in the HL-2A discharges. The SMBI influence time τ_I in the KSTAR discharges was at least order of one longer than that for HL-2A. The analysis to explain the observed difference of τ_I between two devices is progressing. The mitigated ELMs were obtained with slight degradations of confinements in plasma current, stored energy, and toroidal rotation. The diffusive bi-stable cellular automata model well explained the ELM mitigation mechanism by the shallow particle deposition along with the degraded confinements. In 2011, the SMBI experiments were mainly devoted to the effect of shallow particle deposition with its role in the turbulence spectrum change. We will further investigate the deposition depth effect by cryogenic SMBI and the radiative cooling effect by impurity injection.

The preliminary result of vertical jogs on DN shaped discharges presented two issues. The first issue is the up-down asymmetry in ELM triggering. It is likely that ELM triggering by vertical jogs has a preferred plasma configuration between LSN and USN. The other is the multiple ELM triggering observed in large vertical excursions. The observed multiple ELMs might have different triggering mechanisms among them such as edge current, edge pressure, and also equilibrium changes depending on the phase of the vertical jog. In order to tackle the first issue, various configurations including an unfavorable SN configuration will be tested in the next campaign. For the second issue, we will focus on finding the differences such as ELM precursors or filament structures among multiple ELMs based on the measurements such as Mirnov coils and ECEI.

Edge heating by ECH just demonstrated potential capability for affecting edge pedestals. By applying 0.9 MW heating on the edge pedestal, the frequency of ELMs was increased almost factor of two although ΔW_{ELM} was roughly the same before and during ECH. Moreover, accompanying degradations by the edge heating were also observed in particle (line averaged density) and momentum (core toroidal rotation) confinements. To achieve ELM suppression/mitigation, optimized current drive on the edge pedestal needs to be performed. The Ohkawa current drive (OKCD) method has been considered as a solution for the edge current drive since the efficiency of the OKCD method is increased as the trapped population of electrons grows [43].

As mentioned in the above, various control methods were proven to be effective. Moreover, synergy effects among the ELM control methods need to be investigated as well. For instance, it was reported that both the NA field perturbation and the SMBI could mitigate ELMs by altering the type of ELMs although the detailed physics mechanisms might not be same. Therefore, it is beneficial to study a possibility of ‘further mitigation by the SMBI’ of ‘already mitigated ELM state by the NA field perturbation’ for achieving the required level of ELM mitigation for ITER. This might not be fulfilled by individual ELM control methods.

Acknowledgements

The authors deeply appreciate to Dr. England for his valuable advice to make this article much clearer. This work was supported by the KSTAR project funded by the Ministry of Education, Science and Technology of Korea (MEST) and the World Class Institute (WCI) Program of the National Research Foundation of Korea (NRF) funded by the MEST (NRF Grant Number: WCI 2009-001).

References

[1] Wagner F. *et al*., Phys. Rev. Lett. **49** (1982) 1408.
[2] Wagner F. *et al*., Plasma Phys. Control. Fusion **36** (1994) A61.
[3] ITER Physics Editors *et al*., Nucl. Fusion **39** (1999) 2137.

[4] ITER Physics Editors *et al*., Nucl. Fusion **47** (2007) S1.
[5] Connor J.W., Plasma Phys. Control. Fusion **40** (1998) 191.
[6] Wilson H.R. *et al*., Phys. Plasmas **6** (1999) 1925.
[7] Kukushkin A.S. *et al*., Fus. Eng. Design **65** (2003) 355.
[8] Burrell K.H. *et al*., Phys. Plasmas **8** (2001) 2153.
[9] Saibene G. *et al*., Nucl. Fusion **45** (2005) 297.
[10] Oyama N. *et al*., Plasma Phys. Control. Fusion **48** (2006) A171.
[11] Evans T.E. *et al*., Phys. Rev. Lett. **92** (2004) 235003.
[12] Degeling A.W. *et al*., Plasma Phys. Control. Fusion **45** (2003) 1637.
[13] Lang P.T. *et al*., Nucl. Fusion **43** (2003) 1110.
[14] Suttrop W. *et al*., Phys. Rev. Lett. **106** (2011) 225004.
[15] Lee G.S. *et al*., Nucl. Fusion **40** (2000) 575.
[16] Jeon Y.M. *et al*., "Aspects and Applications of Non-Axisymmetric Coils on KSTAR", Proceedings of the 16th Workshop on MHD Stability Control, San Diego, USA, November 21 (2011) and Jeon Y.M. *et al*., submitted to Phys. Rev. Lett (2012).
[17] Xiao W.W. *et al*., submitted to Nucl. Fusion (2012).
[18] Xiao W.W. *et al*., "First Experiments on ELM mitigation by SMBI in HL-2A and KSTAR", Proceedings of the 13th H-mode workshop, Oxford, UK, October 10-12, (2011) and Xiao W.W. *et al*., submitted to Phys. Rev. Lett (2012).
[19] Decker J., "ECCD for Advanced Tokamak Operations Fisch-Boozer versus Ohkawa Methods", Proceedings of the 15th Topical Conference on Radio Frequency Power in Plasmas, Moran, Wyoming, May 19–21 (2003) and
http://www.psfc.mit.edu/library1/catalog/reports/2000/03ja/03ja017/03ja017_full.pdf
[20] Oyama N. *et al*., Nucl. Fusion **51** (2011) 033009.
[21] Herrmann A., Plasma Phys. Control. Fusion **44** (2002) 883.
[22] Lang P.T. *et al*., Nucl. Fusion **36** (1996) 1531.
[23] Lang P.T. *et al*., Nucl. Fusion **51** (2011) 033010.
[24] Lang P.T. *et al*., Plasma Phys. Control. Fusion **46** (2004) L31.
[25] Ahn J-W. *et al*., "Confinement and power threshold study in KSTAR H-mode plasmas", Proceedings of the 13th H-mode workshop, Oxford, UK, October 10-12, (2011).
[26] Ahn J-W. *et al*., submitted to Nucl. Fusion (2012).
[27] Zohm H. *et al*., Plasma Phys. Control. Fusion **38** (1996) 105.
[28] Kim H.K. *et al*., Fus. Eng. Design **84** (2009) 1029.
[29] Schaffer M.J. *et al*., Nucl. Fusion **48** (2008) 024004.
[30] Yun G.S. *et al*., Phys. Rev. Lett. **107** (2011) 045004.

[31] Yun G.S. *et al*., "Two-dimensional imaging of edge-localized filaments in KSTAR H-mode plasmas", Proceedings of the 53rd Annual Meeting of the APS Division of Plasma Physics, Salt Lake City, USA, November 18 (2011) and http://meetings.aps.org/Meeting/DPP11/Event/157736
[32] Liang Y. *et al*., Phys. Rev. Lett. **98** (2007) 265004.
[33] Lang P.T. *et al*., Nucl. Fusion **48** (2008) 095007.
[34] Hill K.W. *et al*., "Progress in X-Ray Imaging Crystal Spectrometer (XICS) Development and Measurements of Ion-Temperature and Flow-Velocity Profiles in Tokamaks and Stellarators", Proceedings of 38th EPS Conference on Plasma Physics, Strasbourg, France, June 27-July 1 (2011) and http://ocs.ciemat.es/EPS2011PAP/pdf/P2.055.pdf
[35] Nam Y.U. *et al*., "Installation and Analysis of First Results of the KSTAR Trial Beam Emission Spectroscopy System", Proceedings of 2011 Fall Meeting of the Korean Physical Society, Busan, Korea, October 19 (2011) and http://www.kps.or.kr/home/kor/symposium/abstract/abstract_view.asp?auid={CBD9F42C-15EE-4975-B9BF-D499C1A8EB65}&globalmenu=3&localmenu=7
[36] Rhee T. *et al*., Phys. Plasmas **19** (2012) 022505.
[37] Gruzinov I. *et al*., Phys. Rev. Lett. **89** (2002) 25; Gruzinov I. et al., Phys. Plasma, **10** (2002) 569.
[38] Kim S.H. *et al*., Plasma Phys. Control. Fusion **51** (2009) 055021.
[39] Hahn S.H. *et al*., Fus. Eng. Design **84** (2009) 867.
[40] Park Y.S. *et al*., Nucl. Fusion **51** (2011) 053001.
[41] Matsuda K. IEEE Tran. Plasma Sci. **17** (1989) 6.
[42] Yoon S.W. *et al*., Nucl. Fusion **51** (2011) 113009.
[43] Ohkawa, T., General Atomic Report no. 4356.007.001 (1976).
[44] Fenstermacher M. E. *et al*., Phys. Plasmas **15** (2008) 056122.

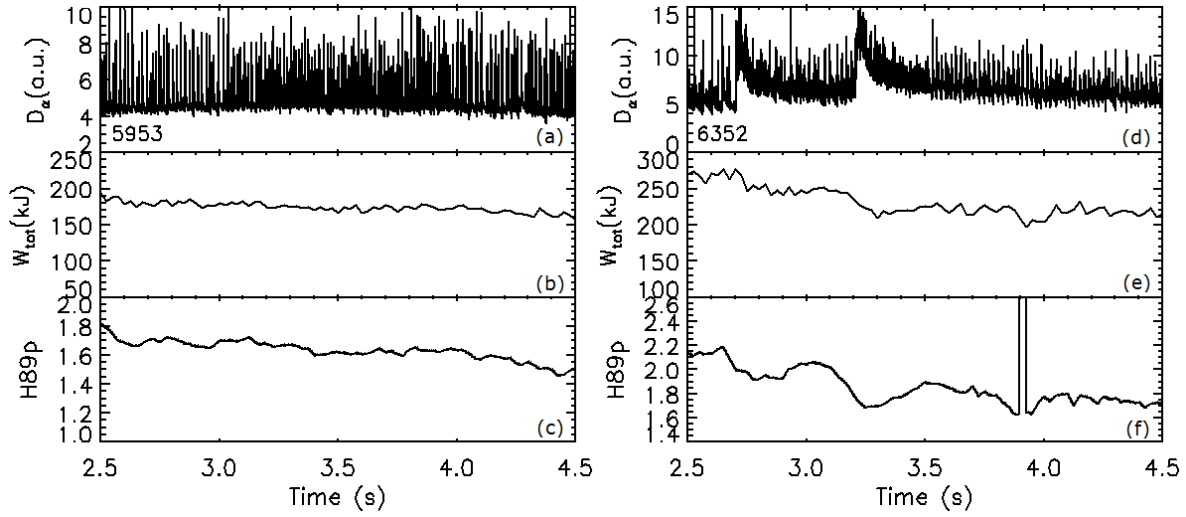

Figure 1. Characteristics of reference discharges for the NA field perturbation (#5953) and the SMBI (#6352). (a) and (d) Temporal evolution of the D_α signal. (b) and (e) The stored energy obtained by EFIT reconstruction. (c) and (f) The confinement enhancement factor H_{89p}. Note that large D_α increases in (d) were caused by the SMBI pulse injections. The stored energy in (e) and the H_{89p} factor in (f) were initially high (H_{89p} >2) before t=2.7 s and dropped by the successive SMBI pulse injections.

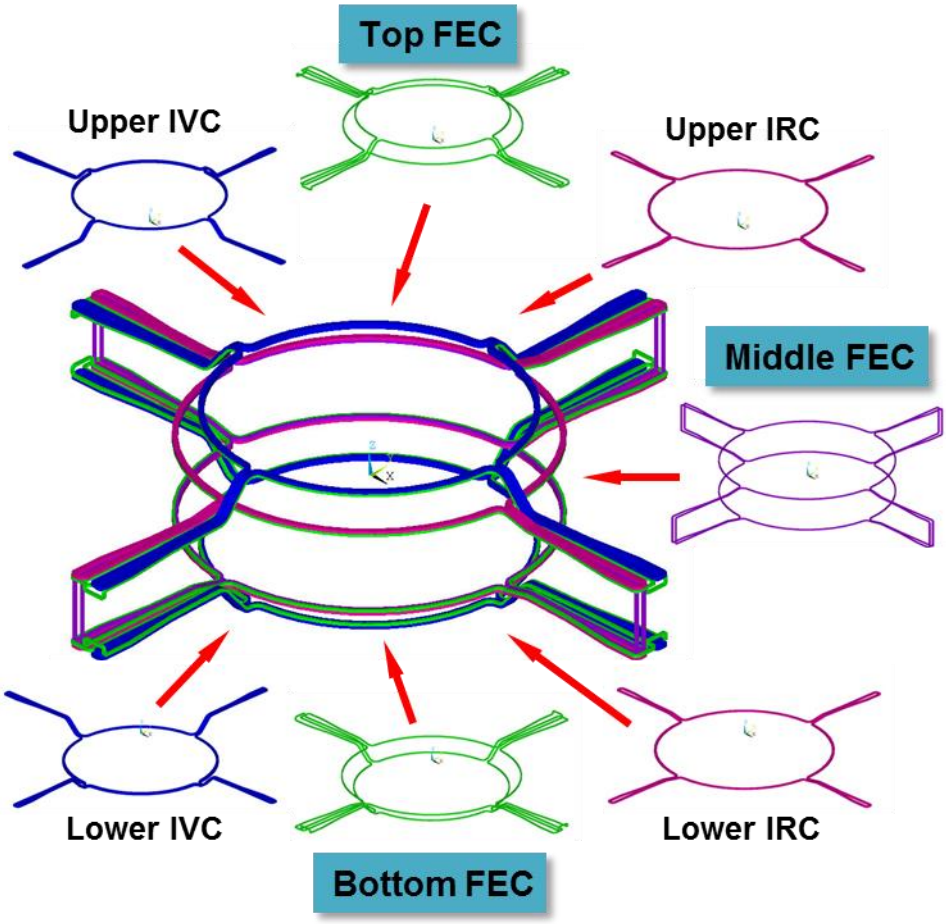

Figure 2. Schematic view of KSTAR IVCC.

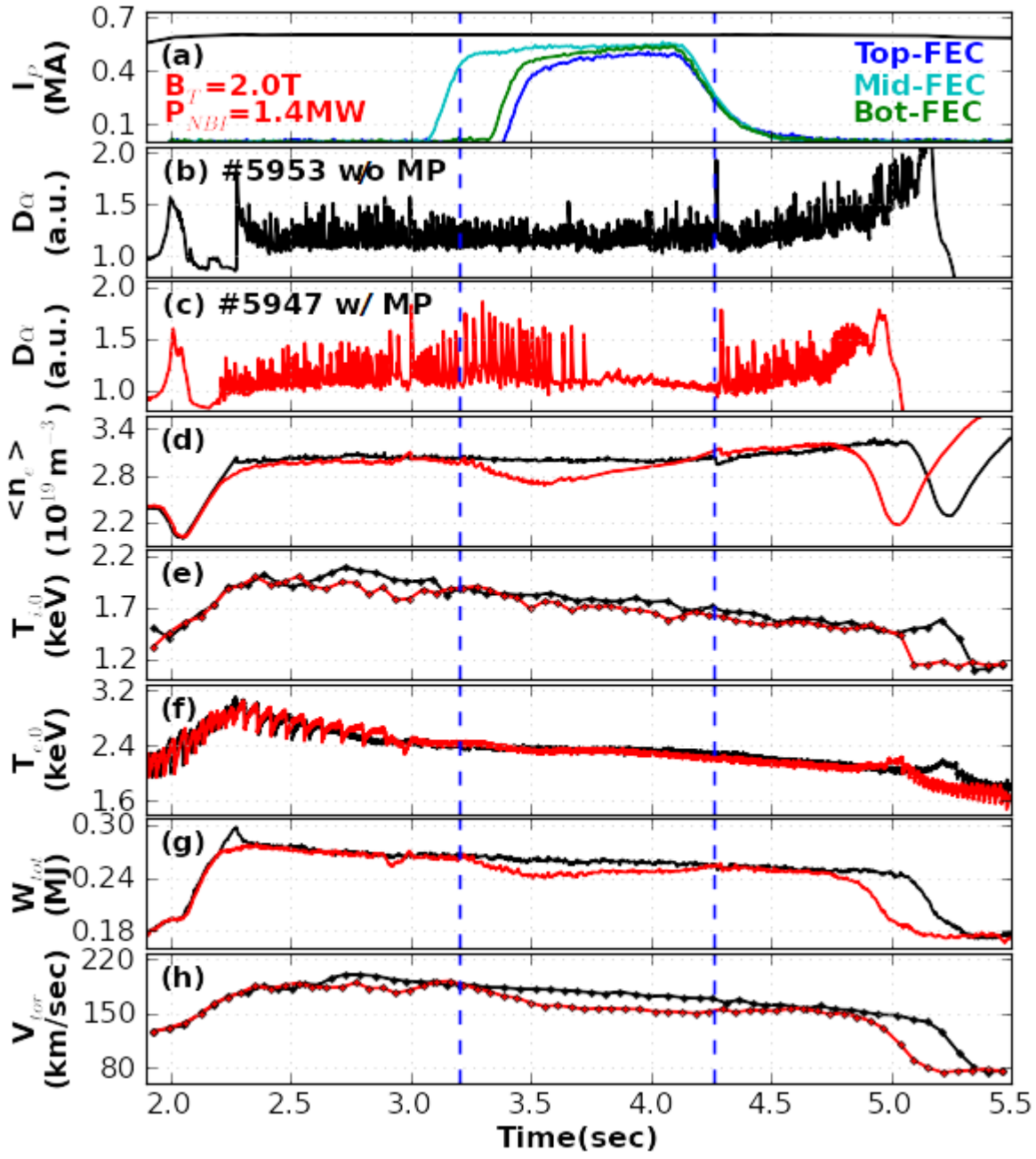

Figure 3. ELM suppression result by applying an n=1, +90 phasing NA field: black line (#5953) and red line (#5947) [16]. (a) Plasma current and FEC (RMP) coil currents during discharge #5947. (b) D_α signal near divertor for the reference discharge #5953. (c) D_α signal near divertor for the ELM suppression discharge #5947. (d) Line-averaged densities. (e) Core ion temperatures. (f) Core electron temperatures. (g) Stored plasma energies. (h) Core toroidal rotations.

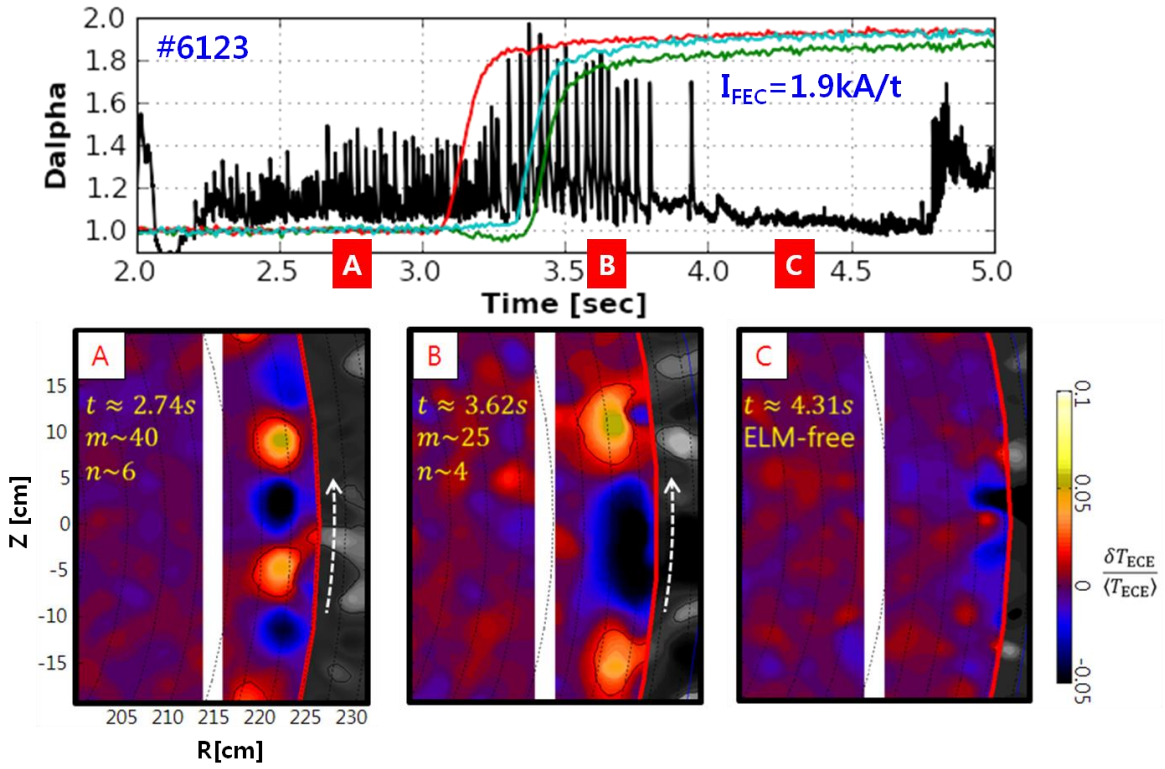

Figure 4. ECEI pictures for different ELM phases [31]. *A*: intrinsic ELM phase, *B*: intensified ELM phase, and *C*: suppressed ELM phase at the times depicted in the upper box. Note that the filament structures in A and B are much different.

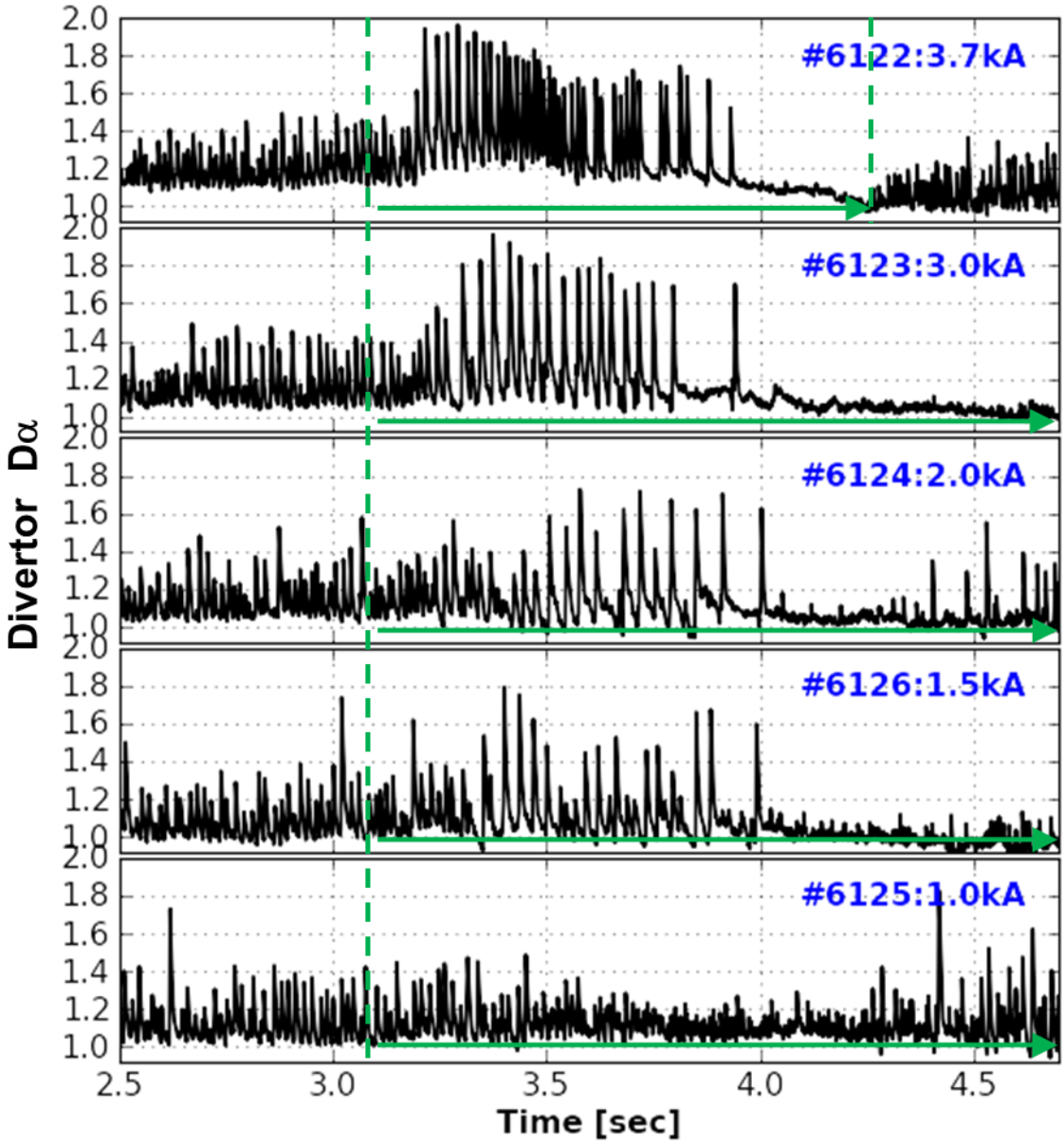

Figure 5. FEC coil current scan to identify the threshold current level for ELM suppression in *n*=1, +90 poloidal phasing [16]. The dotted vertical line depicts the turn-on time of the FEC coils and the duration of FEC coil current is shown by a horizontal arrow for each case.

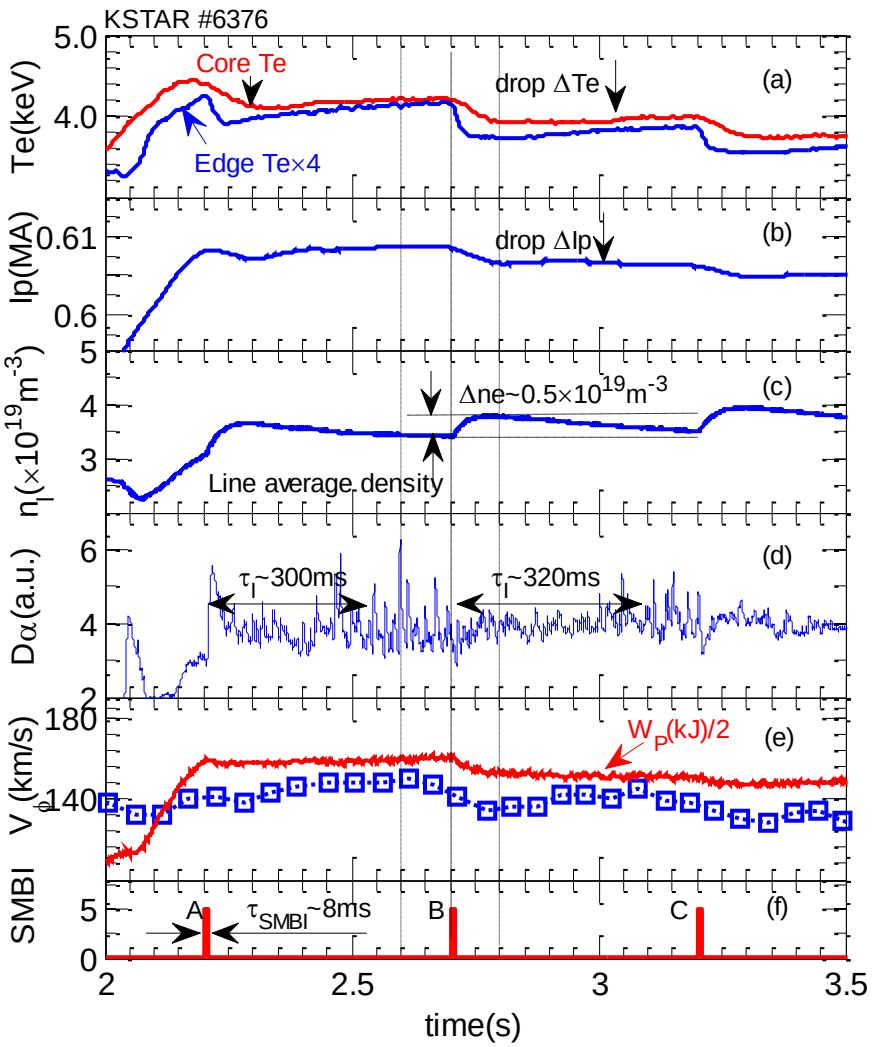

Figure 6. ELM mitigation result by SMBI pulses [18]. (a) The plasma core and edge temperature. The edge temperature decrease rate is faster than that in the core plasma. The plasma current I_p and line-averaged density n_l are in (b) and (c). The density increase Δn_e~0.5x10^{19} m^{-3}. (d) D_α signal. τ_I can be maintained for several hundred miliseconds as shown by the double arrows. (e) The measured time-evolution of the plasma toroidal rotation with the stored plasma energy. For each pulse injection, the plasma toroidal rotation decreases. The order of the SMBI injections is shown in (f). Three pulses A, B and C (τ_{SMBI} ~8 ms, 1 MPa) are injected at 2.2 s, 2.7 s and 3.2 s, respectively.

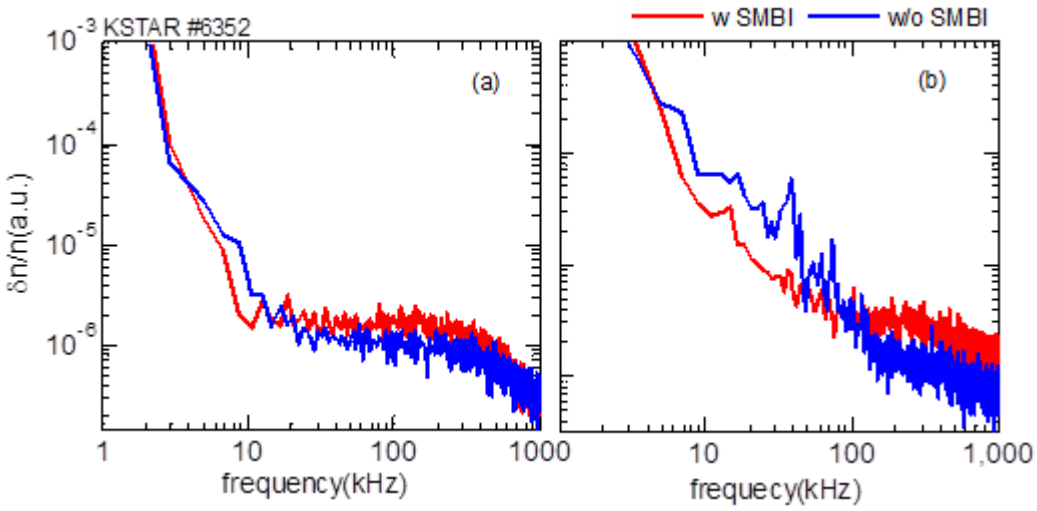

Figure 7. The density fluctuation measured by BES at two different positions [18]. (a) Near the top of the pedestal. (b) Outside of the half pedestal width. Note that high frequency fluctuations increase after the SMBI but low frequency fluctuations decrease in (b). The fluctuations in (a) are almost same before and after the SMBI.

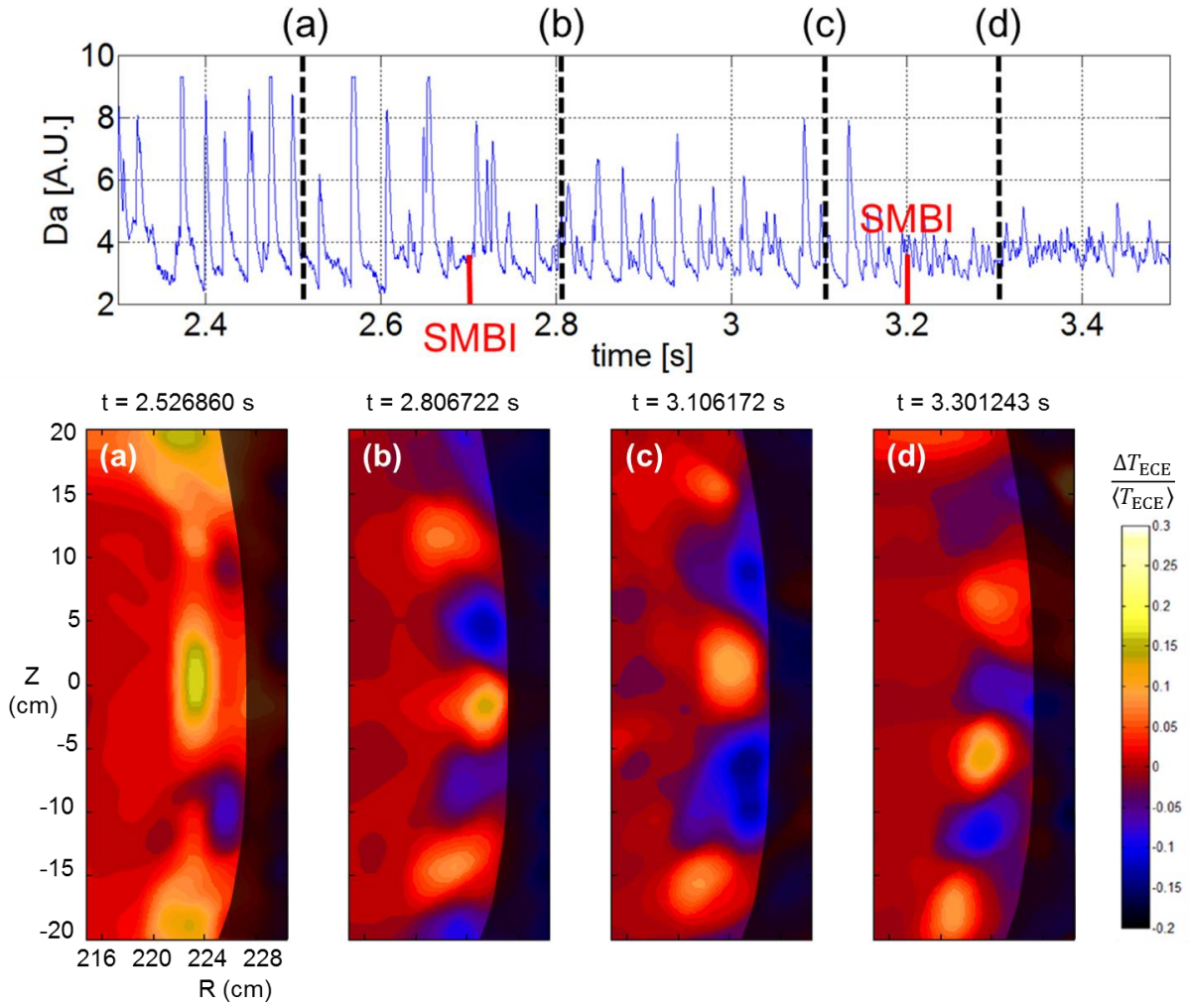

Figure 8. ECEI images of saturated edge filaments [30] prior to the ELM crash [18]. Upper: D_α signal with the SMBI pulse timing. (a) 'before SMBI', (b) '~0.1 s after the 1st SMBI', (c) '~0.4 s after the 1st SMBI', and (d) '~0.1 s after the 2nd SMBI'. The filament amplitude and the distance between the filaments are decreased by SMBIs. The filament amplitude increases slowly until the 2nd SMBI. The arrows indicate the apparent poloidal rotation of the filaments (~2km/s) in the electron diamagnetic direction. In each figure, the far edge region has been grayed out, where the ECEI measurement is difficult to interpret due to the low optical depth.

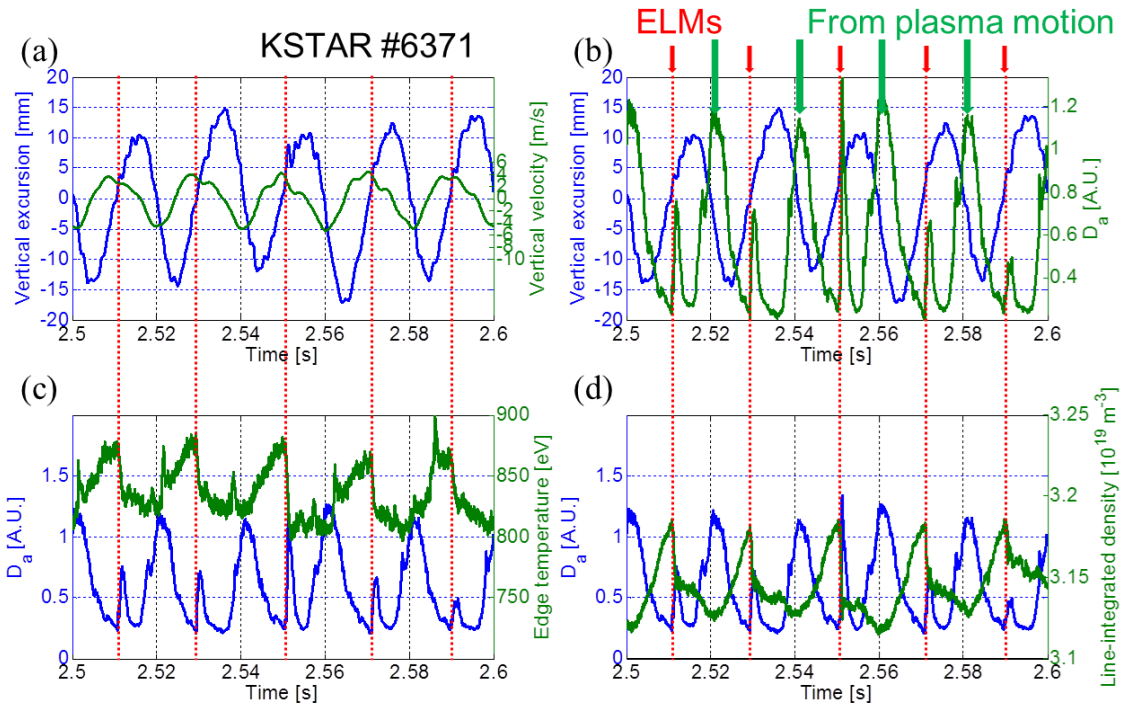

Figure 9. ELM triggering by moderate vertical jogs. (a) Vertical excursion (blue line) and vertical velocity (green line). (b) Vertical excursion (blue line) and D_α signal (green line). Red dotted lines and red arrows represent ELM trigger times. Broad peaks in D_α signal come from plasma motion rather than ELM bursts. (c) D_α signal (blue line) and edge temperature (green line). (d) D_α signal (blue line) and line-averaged density (green line).

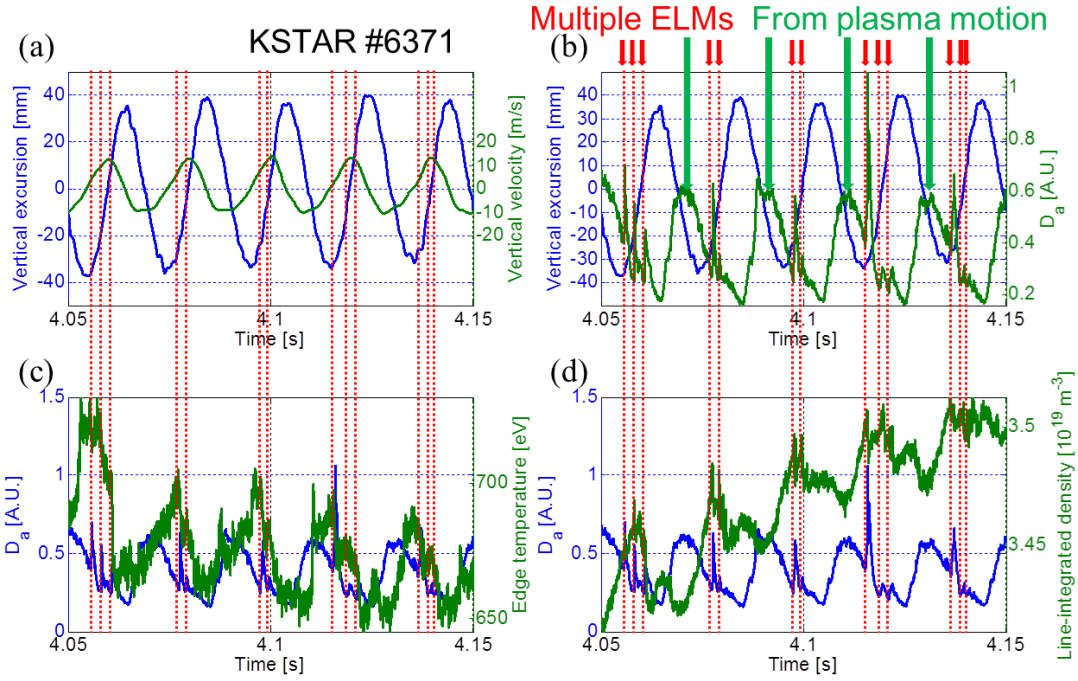

Figure 10. *Multiple* ELM triggering by large vertical jogs. (a) Vertical excursion (blue line) and vertical velocity (green line). (b) Vertical excursion (blue line) and D_α signal (green line). Red dotted lines and red arrows represent ELM trigger times. Broad peaks in D_α signal come from plasma motion rather than ELM bursts. (c) D_α signal (blue line) and edge temperature (green line). (d) D_α signal (blue line) and line-averaged density (green line).

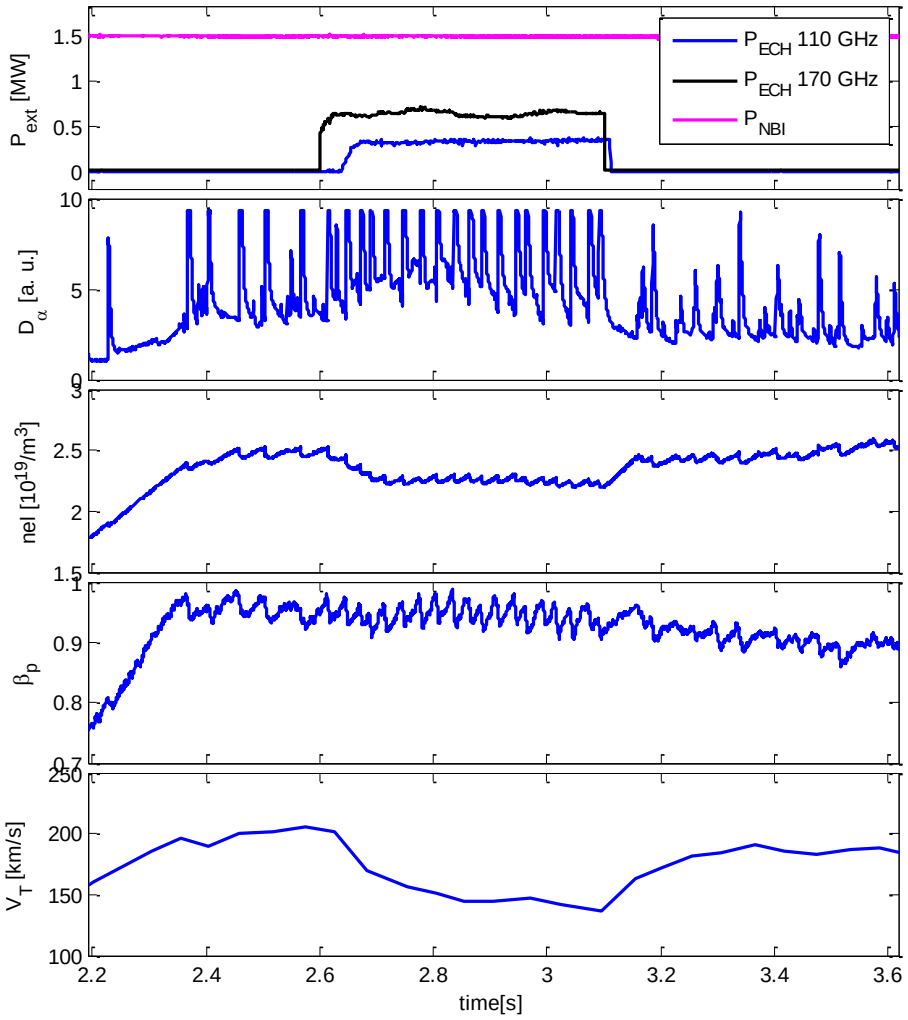

Figure 11. Time-trace of ELM characteristics during the pedestal ECH injection.

Poloidal phasing	**Stochastic region (σ_{CH}>1)**	**Effect on ELM characteristics**
+90 phasing	0.27	Suppression
0 phasing	0.08	Mitigation
-90 phasing	0.04	Intensification
180 phasing	0.22	H-L back transition and locking
Midplane only	0.17	Intensification

Table 1. Summary of ELM characteristics depending on poloidal phasing of applied n=1 NA field. The stochastic region [44] in normalized poloidal flux, ψ_N depicts the width of edge region where Chirikov criterion for stochasticity is satisfied.